Flexible Learning-Free Segmentation and Reconstruction for Sparse Neuronal Circuit Tracing

Ali Shahbazi[1,+], Jeffery Kinnison[1,2,+], Rafael Vescovi[2,3], Ming Du[4], Robert Hill[5], Maximilian Jösch[6], Marc Takeno[7], Hongkui Zeng[7], Nuno Maçarico da Costa[7], Jaime Grutzendler[5], Narayanan Kasthuri[2,3], and Walter J. Scheirer[1,*]

[1]Department of Computer Science and Engineering, University of Notre Dame, Notre Dame, IN, USA
[2]Center for Nanoscale Materials, Argonne National Laboratory, Lemont, IL, USA
[3]Department of Neurobiology, University of Chicago, Chicago, IL, USA
[4]Department of Materials Science and Engineering, Northwestern University, Evanston, IL, USA
[5]Department of Neurology, Yale University, New Haven, CT, USA
[6]Neuroethology Group, IST Austria, Klosterneuburg, Austria
[7]Allen Institute for Brain Science, Seattle, WA, USA
[*]walter.scheirer@nd.edu
[+]These authors contributed equally to this work.

ABSTRACT

Imaging is a dominant strategy for data collection in neuroscience, yielding 3D stacks of images that can scale to petabytes of data for a single experiment. Machine learning-based algorithms from the computer vision domain can serve as a pair of virtual eyes that tirelessly processes these images to automatically construct more complete and realistic circuits. In practice, such algorithms are often too error-prone and computationally expensive to be immediately useful. Therefore we introduce a new fast and flexible learning-free automated method for sparse segmentation and 2D/3D reconstruction of brain micro-structures. Unlike supervised learning methods, our pipeline exploits structure-specific contextual clues and requires no extensive pre-training. This approach generalizes across different modalities and sample targets, including serially-sectioned scanning electron microscopy (sSEM) of genetically labeled and contrast enhanced processes, spectral confocal reflectance (SCoRe) microscopy, and high-energy synchrotron X-ray microtomography (μCT) of large tissue volumes. Experiments on newly published and novel mouse datasets demonstrate the high biological fidelity and recall of the proposed pipeline, as well as reconstructions of sufficient quality for preliminary biological study. Compared to existing supervised methods, it is both significantly faster (up to several orders of magnitude) and produces high-quality reconstructions that are robust to noise and artifacts.

Introduction

The ability to comprehensively study the brain is within reach. Advances in tissue preparation and imaging technologies have allowed researchers to collect vast amounts of targeted structural data, potentially enabling new multi-resolution, multi-modal studies of neural volumes. Brain imaging techniques from microscopy such as serially-sectioned scanning electron microscopy (sSEM), high-energy synchrotron X-ray microtomography (μCT), and spectral confocal reflectance (SCoRe) microscopy provide high-quality images with nanoscale or single-neuron resolution.

Along with improvements to image quality, next-generation imaging technologies are also producing data at a faster rate than ever before. In 2013, the Allen Brain Institute produced 750 gigbytes of raw two-photon microscopic images in 18 hours[1]. Currently, new multi-beam scanning electron technologies only require 2.5 hours to generate the same amount of raw data[1]. This increase in imaging speed has led to a neuroscientific data explosion, however the systems for processing, analyzing, and visualizing regions of interest in these datasets has not kept pace.

Segmentation and reconstruction efforts are often carried out manually on small neural image volumes or over limited subsets of larger volumes. This process is time consuming, however, and becomes infeasible for large volumes. For example, in one study conducted by the Max-Planck Institute of Neurobiology, over the course of 8 weeks 13,000 EM images, each 2.5 gigapixels in size, were acquired[1]. The subsequent manual segmentation and reconstruction efforts led to a validated model of a 900-neuron connectome. But it required two years to be completed. Such an endeavor is clearly not scalable and is intractable to be carried out for every imaged neural volume.

With respect to approaches for generating manual annotations, a number of software frameworks are available, including Eyewire[2], D2P[3], Mojo[4], Catmaid[5], KNOSSOS[6], Ssecrett[7], TrakEM2[8] and ITK-SNAP[9]. Some connectomics studies are based

on exhaustive manual proof-reading of results from an algorithm[10,11], which, like the creation of ground-truth data, is not practical for data sets consisting of high resolution images or large volumes. For example, Takemura *et al.*[10] described how the reconstruction of a relatively small volume of *Drosophila* brain required $\sim 12,940$ person-hours of proof-reading.

To overcome the limitations of manual annotation, expert-verified reconstructions may be used to train machine learning models to perform automatic segmentation and reconstruction. A wide variety of methods — highly dependent on supervised machine learning — exist for the dense EM segmentation and reconstruction problem. The methods include SVM-based algorithms[12–16], Random Forests[12,17–24], Conditional Random Fields[22], and Artificial Neural Networks[25–30] (*i.e.*, deep learning). These machine learning approaches can be found in popular software packages for connectomics image analysis such as Rhoana[31] and Ilastik[18,19,32]. In addition to traditional neural network-based approaches, research into fully-convolutional networks for image segmentation related to microscopy produced the U-Net[33] architecture. This type of network uses convolutions, downsampling, and upsampling in a U-shaped configuration to home in on features and good candidate output segmentations. Additionally, intermediate results from the downsampling side of the network are fed to the corresponding convolutional units on the upsampling side to provide extra information to later layers. These networks have been applied to both the dense[34] and sparse[34,35] segmentation problem in the 3D domain.

In spite of these machine learning innovations, neuroscientists must remain in-the-loop when applying deep learning methods to provide high-quality training data. Images from neuroscience experiments are complex, containing a wide variety of cells and other micro-structures that may only be reliably and correctly identified by expert annotators. This is not a good scenario for deep learning methods, which require a prohibitively large amount of annotated training data. For example, in a study by Chklovskii et al.[36], manual segmentation of a stack of electron microscopy images at a resolution of 4000×4000 pixels required two person-years. Similarly, Helmstaedter *et al.*[6] estimated that the time needed for contouring neurites of length 0.3m is 30 person years (around $60,000$ hours). Even in the presence of training data, deep learning methods do not generalize well to new datasets and require re-training, which in-turn requires more expert annotations.

Even if an image volume has been annotated, deep learning methods require a vast amount of specialized computational resources. Neural networks can take weeks or months to train, and feature extraction, while faster than training, is still inefficient even on a graphical processing unit (GPU). For just 100 images with a resolution of 1024×1024, a state-of-the-art network for connectomics takes 59 hours for training and evaluation[29].

Given the limitations of deep learning for neural circuit reconstruction, it is worth re-evaluating the current assumption that machine learning should be indiscriminately applied to all pattern recognition problems. New tissue preparations and imaging techniques have drastically improved the signal-to-noise ratio across imaging modalities, thus automated segmentation and reconstruction methods for neural circuit tracing can now look to reduce manual and computational overhead by exploiting geometric and grayscale intensity cues with classical image processing, removing training entirely.

Here we introduce the Flexible Learning-Free Reconstruction of Neural Circuits pipeline (FLoRIN) for automatic segmentation and reconstruction (see: Methods). In contrast with supervised and unsupervised machine learning methods, FLoRIN segments and reconstructs neural volumes using classical, learning-free computer vision techniques in 2D or 3D. Figure 1 provides an overview of the FLoRIN pipeline. This method distinguishes itself from other segmentation and reconstruction efforts by a number of facets:

- **Learning-free segmentation.** High-quality images can be segmented using classical image processing and computer vision methods that eliminate the need for expensive and slow manual annotation for machine learning. Under this regime, image analysis for microscopy becomes a collaborative process between neuroscientists and computer vision experts, allowing for methodological advances in both fields. Along these lines, we introduce the Local Adaptive Thresholding (LAT) method, which exploits local image data in 2D or 3D to quickly and accurately binarize images with only a single tunable parameter.

- **Real-time segmentation.** Learning-free computer vision methods incur less computational overhead than machine learning methods, allowing for real-time segmentation of neural volumes as they are imaged. We compared the running time of FLoRIN with that of a fully convolutional neural network, 3D U-Net[34] as well as previous work in EM sparse reconstruction[37], and achieved high quality results in remarkably short time-frames.

- **Multi-modal image segmentation.** Most neural image segmentation and reconstruction approaches are designed to work with a single imaging modality, either because of training limitations or because of the use of modality-specific features. Our pipeline is easily adapted to multiple modalities, including sSEM[38], SCoRe[39], and μCT X-ray imaging, with only minor changes to the parameterization.

- **Operates on subsets of data.** Neural image data can be prohibitively large, forcing researchers to operate only on small subsets at a time. Our methodology is able to operate on subsets of images and volumes, breaking them down into "tiles" that may be segmented independently and recombined for reconstruction. Tiling reduces memory consumption, enables

parallel computation, and limits the effects of grayscale shifts that would otherwise have a large impact on the grayscale distribution.

- **Sparse reconstruction vs. dense reconstruction.** Special tissue preparations can enhance the contrast of specific cell types[37], and certain imaging techniques can selectively highlight specific anatomical structures[40]. These methods lead to a sparse reconstruction problem, which is much faster to solve than the exhaustive dense reconstruction problem, and provides useful results for multi-modal image reconstruction problems (*e.g.*, co-registration of different types of microscopy) and cell-specific studies[10,11,41]. Further, techniques in this vein can take advantage of the morphological characteristics of known cell types. Dense reconstruction may still be possible with some methods facilitating sparse reconstruction, but is not always necessary.

- **Enables reproducible science.** All operations carried out by FLoRIN are deterministic, as opposed to learning methods that introduce stochasticity into computations. With a given parameterization, FLoRIN will always produce identical segmentations and reconstructions of a given dataset.

- **Provides microstructure statistics.** During the segmentation process, spatial, geometric, and grayscale data are extracted from discovered microstructures to identify them. This information is stored in a database along with a statistical report that includes microstructure-specific information such as the size distribution, spatial density, and proximity to other microstructures. This information can be re-computed over local areas to study specific regions of the brain.

- **Minimal user intervention.** Our proposed approach does not require a human in the loop to make extensive corrections as in prior studies[21,30]. Instead, a small number of tunable parameters — one for binarization and between one and five for microstructure identification — must be set before segmentation based on a tissue quality assessment.

FLoRIN is dramatically faster than deep learning methods, more tolerant to noise and image artifacts, and generalizable across datasets and modalities. To demonstrate the improvements made possible by FLoRIN, we segment and reconstruct two μCT X-ray volumes, two sSEM volumes, and one SCoRe volume. Where ground-truth annotations are available, we compare the results of FLoRIN against 3D U-Net[34], a state-of-the-art fully convolutional neural network designed to segment neural volumes. In every case, FLoRIN produces higher-quality reconstructions than 3D U-Net in a fraction of the time without training. We conclude that our pipeline is suitable for sparse segmentation and reconstruction of both *in-vivo* and *ex-vivo* imaging modalities.

Results

We applied FLoRIN to sparsely segment and reconstruct neural volumes from three different modalities: μCT X-ray, sSEM, and SCoRe. Two of the image volumes were expert-annotated, and in these cases we also trained a 3D U-Net model to compare FLoRIN against a state-of-the-art deep learning model designed for microscopic image segmentation. In the following analyses, we denote FLoRIN using 2D Segmentation and 2D Filtering as "2D FLoRIN" and FLoRIN using 3D Segmentation and 3D Filtering as "3D FLoRIN".

Practically speaking, the only difference between the two methods is that 2D FLoRIN operates over single images at a time, while 3D FLoRIN operates over volumes at a time. Operating in 3D allows FLoRIN to account for volumetric information and improve the quality of its results, however operating in 2D allows FLoRIN to ignore localized artifacts and interpolate over missing image data or removed artifacts. The modular nature of the FLoRIN pipeline allows for the Segmentation, Identification, and Reconstruction stages to operate independently in either 2D or 3D.

μCT X-ray Volumes

X-ray computed tomography is an imaging technique that captures volumetric views tissue samples samples. Since the contrast mechanism is directly related to the sample density, it is possible to distinguish between macrostructures like cells, myelinated bundles and vasculature. We examine two such μCT X-ray volumes imaged at micron-scale resolutions. In this study, two different μCT image volumes were reconstructed: a standard rodent brain volume (SRB) with human-generated annotations and an APEX2-labeled rodent brain volume (ALRB) that includes APEX2-labeled cells.

Standard Rodent Brain

The SRB volume is relatively small, spanning only a $300 \times 300 \times 100$ voxel region imaged at a resolution of 1.2μ[40]. But it is accompanied by a partial annotation of the imaged cells, making it suitable as a benchmark for automatic segmentation and reconstruction methods. Cells and vasculature may be visually differentiated (Figure 2 Panels A & B), however automatic segmentation is complicated by grayscale shifts and cells that are within close proximity of each other, which can both lead to merge errors and voxel mis-classifications. Without careful consideration of these factors or extensive training, automated

methods will fail to properly segment the cells and vasculature. With this in mind, we created reconstructions of the cells and vasculature in SRB using 2D FLoRIN, 3D FLoRIN, and 3D U-Net.

Of the three methods, 3D FLoRIN produced the reconstruction closest to the expert annotations. As shown in Table 1, the 3D FLoRIN reconstruction was a Hausdorff Distance (Supplementary Methods: Evaluation Metrics) of 1.59×10^{-3} from the ground-truth. The 3D U-Net and 2D FLoRIN reconstructions were factors of five and six farther from the ground-truth than the 3D FLoRIN reconstruction, respectively. All three methods achieved 100% recall, discovering all 313 annotated cells. An additional seven cells were also discovered and verified, raising the total number segmented to 320.

Qualitatively, all three reconstructions capture the morphology of the cells and vasculature well. As seen in Figure 2 Panels D & E, the cells are all smooth, localized structures while the vasculature segments weave and branch through the volume as connected tube-like structures. When superimposed in 2D (Supplementary Figure S3), the segmented areas visually correspond well with the original images, contrasting with the manual annotations which only capture a subset of cells and are (surprisingly) not faithful to the visible structures in the images. Despite the fact that the expert annotations only capture cells in SRB, both FLoRIN methods segmented both cells and vasculature simultaneously. 3D U-Net could not be trained on vasculature in this volume and only segmented the cells. FLoRIN is thus able to extract useful information from images that human annotators may exclude or overlook due to time constraints.

In addition to the high-quality reconstructions, both versions of FLoRIN offer a speedup of several orders of magnitude over 3D U-Net by virtue of eliminating the training step. Whereas the total time to train and segment with 3D U-Net was 10,364.4 s, 2D FLoRIN completed the same task in 9 s with similar results, and 3D FLoRIN did so in 19.2 s with significantly better results. Moreover, both versions of FLoRIN required only a single CPU to segment and reconstruct SRB, however 3D U-Net required a high-end GPU to train in a tractable amount of time. Thus, FLoRIN is less computationally intensive than 3D U-Net and requires no special hardware to operate effectively.

APEX2-Labeled Rodent Brain

The ALRB dataset (Figure 2 Panel F) is much larger than SRB, consisting of a $3948 \times 1858 \times 534$ voxel volume imaged at a resolution of 1.2μ, which encompasses a coronal section of the rodent brain. To prepare this sample an 81 day old mouse was transcardially perfused with 4% paraformaldehyde, 2.5% glutaraldehyde in a 0.1 M sodium phosphate buffer solution. A $300\,\mu$m coronal slice was prepared on a vibratome, reacted with DAB-Ni, then treated with 1% osmium tetroxide for 40 minutes, dehydrated through graded alcohols and acetonitrile as a transitional solvent, then embedded in Durcupan epoxy resin. The detailed protocol is described by Lam *et al.*[42].

In addition to cells and vasculature, this dataset contains APEX2-labeled cells as a third class of structure to segment (Figure 2 Panels G & H). The APEX2-labeling was applied to a subpopulation of layer 4 cells. No ground-truth annotations exist for this volume, making a quantitative evaluation of the reconstructions impossible. We instead report properties of the segmented objects to compare the performance of 2D FLoRIN and 3D FLoRIN.

As shown in Table 2, both FLoRIN methods segmented 123,424 non-APEX2-labeled cells and 1,524 APEX2-labeled cells in ALRB, and the vasculature was segmented as a single connected component. Moreover, the reconstructions created by both FLoRIN methods were a Hausdorff distance of 1.614×10^{-3} apart. These findings indicate that 2D FLoRIN and 3D FLoRIN are able to discover approximately the same information. As seen in Figure 2, the APEX2-labeled cells are visually distinct from the unlabeled cells and vasculature; the Filtering stage of the pipeline is able to distinguish between the two types. Such fine-grained distinctions are possible when the segmentation method is not dependent upon explicit training that may overlook a diversity of relevant features.

sSEM Volumes

Eliminating learning from the segmentation and reconstruction process potentially allows for generalization across different imaging modalities. Whereas the goal of segmenting and reconstructing μCT X-ray volumes is to discover large structures and high-level information about the structure of the brain, sSEM images are of high enough resolution to follow individual processes (Figure 3 Panel A). The dataset introduced by Jösch *et al.*[37] contains APEX2 positive processes with a sample preparation designed to enhance microstructures of interest for automatic sparse segmentation (Figure 3 Panel B). APEX2 labels starburst amacrine cells in the dataset, thus we attempt to reconstruct the associated dendritic branches of these cells (Figure 3 Panels C-F).

Subvolume 1

The first subvolume consists of a $3{,}000 \times 5{,}000 \times 150$ voxel region (4nm/pixel) with substantial accompanying ground-truth annotations (Figure 3 Panel G). This stack was processed with 2D FLoRIN (Figure 3 Panel H), 3D FLoRIN (Figure 3 Panel I), and 3D U-Net to create 3D and 2D reconstructions of the APEX labeled regions, where the 2D reconstruction is the flattened version of the reconstruction that represents all of the segmented structures in a single plane. The 2D reconstruction is useful

when studying SAC cells that are shallow along one dimension of the stack, allowing a unified view of the connections between cells, while a 3D reconstruction preserves depth information.

3D FLoRIN created the closest reconstructions to the ground-truth, as shown in Table 4. The 3D FLoRIN 3D reconstruction was a factor of three closer to the ground-truth than the 3D reconstruction created by 2D FLoRIN, and the 2D reconstructions captured roughly the same information. Once again, including volumetric information in the segmentation process allowed for FLoRIN's learning-free methods to take advantage of additional contextual information to refine the segmentation (*e.g.*, by boosting the signal-to-noise ratio during thresholding, enabling filtering based on feature depth).

3D U-Net was unable to create a meaningful reconstruction of Subvolume 1. While annotations of this dataset exist, training is confounded by artifacts and noise, including non-APEX2-labeled processes in the image. Ultimately, more annotations are needed to properly train 3D U-Net to distinguish between the APEX2 labeled SAC cells and other image features.

Subvolume 2

The second subvolume of the sSEM dataset consisted of 4,500 $\times$ 6,500 $\times$ 190 voxels (4nm/pixel), with large artifacts obscuring APEX2 positive processes, major grayscale shifts, and additional positive segments beyond the ground-truth annotations (Figure 3 Panel K). Once again, the 3D FLoRIN reconstruction was closer to the expert annotations than that of 2D FLoRIN (Figure 3 Panels L-M).

The 2D FLoRIN reconstruction had a final recall of 93.03%, however the reconstruction (Figure 3 Panel L) merges a number of the annotated features. The 3D FLoRIN reconstruction (Figure 3 Panel M), on the other hand, was able to separate microstructures and even discovered APEX2 positive processes overlooked by annotators (Figure 3 Panel N). As with Subvolume 1, 3D U-Net was unable to segment and reconstruct this dataset.

Spectral Confocal Reflectance Microscopy Volumes

With μCT X-ray and sSEM reconstructions, we demonstrated that FLoRIN is capable of reconstructing relevant structures in *ex-vivo* images. To determine if FLoRIN could also be applied to *in-vivo* data we also analyzed high-resolution optical images acquired from the live mouse brain. SCoRe is a recently developed technique that allows for precise label-free imaging of myelin in the live brain and in tissue samples[39]. SCoRe can be combined with fluorescence imaging in order to visualize patterns of myelination along stretches of single axons. In this modality, myelin patterns along single axons are captured by combining SCoRe (Figure 4 Panels C & D) with confocal fluorescence imaging in a transgenic mouse with YFP (Figure 4 Panels A & B) labeling on a subset of axons. FLoRIN was applied to this volume to reconstruct a single myelinated axon from among a large number of visible intersecting axons. 3D U-Net could not be applied to this problem because no annotations exist to train on SCoRe data.

We applied FLoRIN to a $311 \times 66 \times 21 \mu m$ SCoRe volume to reconstruct a single, contiguous myelinated axon. This subset contains a number of other axons that intersect with the axon of interest. Initially, the YFP channel was segmented by 3D FLoRIN (Figure 4 Panel E), and connected components were filtered to remove any unconnected segments (Figure 4 Panel F). Segments from the SCoRe channel were then acquired by only considering those overlapping the segmented portions of the YFP channel (Figure 4 Panel G). The final reconstruction (Figure 4 Panel H) combines the YFP and SCoRe channel segmentations.

In total, 3D FLoRIN revealed two long axons in the web of smaller axons, segmented as two components. Notably, FLoRIN was able to follow both axons over a long distance in the YFP channel, the left part of the axon is not labeled with SCoRe, thus showing the specifity of FLoRIN for identifying overlap. These factors together indicate that FLoRIN reconstructions are able to discover far-reaching processes without training. FLoRIN created this reconstruction in $38.92 s$.

Discussion

To understand the mechanism of neuronal computations, access to high-quality segmentations and reconstructions of neural structures is paramount. FLoRIN demonstrably meets these needs and can do so in a fraction of the time needed to employ learning-based solutions. Whereas U-Net and other deep learning models require large amounts of expert-annotated training data, which is time-consuming and costly to generate, FLoRIN is able to process new data without *a priori* information. This is demonstrated by the reconstructions of the ALRB volume and SCoRe subvolumes, which have no associated manual annotations. Moreover, FLoRIN bypasses the training time required to tune learning-based models by virtue of being learning-free, reducing both the computational time and the overall burden of training a learning model to recognize features of interest.

As our reconstructions show, FLoRIN is able to capture information from images from microscopy that is faithful to expert-annotated ground-truth. In all cases, 3D FLoRIN produces results that are several factors closer to the ground-truth than 3D U-Net trained on the ground-truth is able to produce, and as stated it does so in a fraction of the time. In the case of the SRB volume, the primary advantage of FLoRIN is its speed. In the case of the sSEM volumes, however, 3D U-Net was unable to generate any meaningful results due to the similarity of APEX2 positive structures and other non-APEX-labeled features.

FLoRIN reconstructed the APEX2 positive processes within both subvolumes and successfully filtered out the features that 3D U-Net mistakenly segmented. Thus, FLoRIN outperforms a state-of-the-art deep learning model in multiple modalities.

Another key weakness of deep learning methods is the requirement that models be trained independently on examples of each microstructure to be segmented. FLoRIN, by contrast, is able to segment multiple classes of structures simultaneously: in each of the reconstructed X-ray volumes, the cells and vasculature were segmented in a single pass, and in the ALRB reconstruction APEX2 cells were also captured. In this way we are able to handle segmentation errors, such as merge errors between different classes of microstructure, by applying intermediate watershedding prior to morphological filtering. While there are limitations to the simultaneous multi-class segmentations that arise when microstructures have high contrast with one another, this simply requires re-processing the image volume with a different threshold value or window size.

On top of outperforming U-Net, FLoRIN may be applied to new volumes and new modalities without requiring extensive manual annotations for training. FLoRIN was successfully applied to segmenting a new μCT X-ray volume, creating the first reconstruction of the ALRB volume without any prior information. Additionally, the FLoRIN statistical report provided initial data about the distribution of cells in the ALRB volume. This capability is not limited to previously-processed modalities: FLoRIN also created reconstructions of two SCoRe subvolumes with no prior training, tracing far-reaching myelinated axons with no breaks. That FloRIN was able to successfully reconstruct new volumes and modalities indicates that it is more generalizable than deep learning methods, which would likely require additional training or complete re-training to effectively handle new datasets.

FLoRIN successfully solves the sparse segmentation and reconstruction problems by taking advantage of the inherent properties of sample preparations and by operating on local neighborhoods of voxels. The Local Adaptive Thresholding (LAT) methodology (Supplementary Methods: Local Adaptive Thresholding) employed by FLoRIN is able to focus in on small regions, making it robust to grayscale shifts and distant noise that would otherwise confound global thresholding methods. Moreover, tissue preparation enhances the contrast of features of interest, in turn allowing for a stronger local threshold. LAT can also account for volumetric information, allowing FLoRIN to process neural volumes as *volumes* rather than sequences of images. End-to-end processing in 3D can lead to greater biological fidelity, as demonstrated by the fact that 3D FLoRIN consistently created sparse reconstructions of higher quality than 2D FLoRIN.

Processing neural volumes in 2D can still be useful, for example in the presence of a low signal-to-noise ratio. In this case, Segmentation can be carried out in either 2D or 3D, then the Identification stage can filter out artifacts in 2D, and finally the Reconstruction stage can interpolate single layers of a microstructure that were removed due to merge errors during the Identification stage. While such capability is limited, in the same situation a learning-based model would break down due to an inability to recognize patterns in the noisy images or by virtue of positively identifying artifacts when they are merged with microstructures of interest. FLoRIN allows for a more flexible approach to segmentation under unfavorable conditions.

A surprising result of LAT is that computing it over subvolumes (3D) or image patches (2D) leads to higher-quality results than processing the entire volume at once. This is due to the integral image, which computes a cumulative summation over multiple dimensions in order, for example x- then y- then z-dimension. Computing the integral image over a subvolume, and subsequently computing the average intensity to calculate threshold values, excludes information from distant points (*e.g.*, noise, grayscale shifts) and normalizes threshold values to the local grayscale values. By using a sliding window to choose subvolumes, we are able to perform both the Segmentation and Identification stages of FLoRIN on subsets of the volume at a time and then combine the result in the Reconstruction stage. This result implies that each subvolume may be processed in parallel, opening the door to distributed computing optimizations.

Expert-annotated ground-truth is costly, but necessary to make the best use of deep learning methods. In the absence of such data, we are forced to either accept poor learning models or turn to classical learning-free methods for automated segmentation and reconstruction. As our reconstructions demonstrate, both 3D and 2D FLoRIN outperform deep learning in the data-starved regimes of μCT X-ray and sSEM sparse segmentation by bypassing learning. Learning-free methods are generalizable across imaging modalities because they do not tune to specific features and noise, and so they are suitable for creating candidate reconstructions which may then be validated by experts. We suggest that FLoRIN should be incorporated into sparse segmentation and reconstruction pipelines as a means for preliminary study and semi-automated annotation. Reconstructions created by FLoRIN can be used as a starting point for deciding how to study neural volumes: experts can gain a high-level view and choose regions to study at higher resolutions. Further study is possible by validating FLoRIN reconstructions — for example, examining each segmented microstructure alongside the original images and determining the class of structure it represents — and then training a deep learning model like U-Net on the validated reconstruction. In this way, experts can make full use of the enormous amount of data being generated by new imaging technologies.

Methods

FLoRIN Framework

The FLoRIN pipeline is a new open-source software package[1] for flexible learning-free sparse segmentation and reconstruction of neural volumes. FLoRIN is divided into three stages, each of which use a series of classical image processing methods in either 2D or 3D: the Segmentation stage, Identification stage, and Reconstruction stage.

Stage 1. Segmentation

Starting with a set of raw images of a neural volume, the Segmentation stage adjusts the grayscale histogram of the images and thresholds the result. A number of standard grayscale adjustments are available, including histogram equalization, histogram re-scaling, and Wiener filters. Thresholding is carried out using the Local Adaptive Thresholding (LAT) algorithm described in Supplementary Methods: Local Adaptive Thresholding. Methods in the segmentation stage are applied in 3D by default to take advantage of volumetric context, however FLoRIN may also drop back to 2D if needed (*e.g.*, for performance, to handle inconsistencies in 3D). The result of the Segmentation stage is a binarized version of the raw images that labels potential microstructures of interest.

Stage 2. Identification

The Identification stage takes the binary output of the Segmentation stage and removes small connected components for preliminary artifact filtering. The remaining connected components are then found and filtered into groups based on their geometric and grayscale properties. Connected components can be found in 3D to recover volumetric models directly, or else in 2D and stitched into 3D models. Supplementary Figure 1 provides an overview of the 2D filtering process. Information about the connected components is saved to a database for further review. Details of the resulting statistical report characterizing the anatomy of interest are described below.

Stage 3. Reconstruction

After Identification, FLoRIN saves each class of microstructure into an individual volume in the Reconstruction stage. Volumes can be output in a number of standard file types for compatibility with various postprocessing and rendering software. If a 2D reconstruction is desired, FLoRIN will collapse the computed volumes into a single plane and save the plane to file. Additionally, a statistical report is compiled from the database created during the Identification stage and can be modified to suit the content of the reconstruction.

Statistical Reports

Along with the 3D reconstruction, FLoRIN outputs a Statistical Report that contains spatial, morphological, and grayscale information about each segmented microstructure. In addition to single-microstructure properties such as centroid, bounding box, volume, spatial orientation, and mean grayscale intensity, FLoRIN can compute statistics over groups or classes of microstructures. Such statistical data allows for investigation into microstructure sizes, spatial distribution, or relationships between different classes of microstructure. When evaluating the ARBS dataset, for example, we used the statistical report to compute the total number of discovered cells, average cell size, and average minimum intercellular distance. The statistical report allows for flexibility in how a neural volume is investigated. Often, the imaged volume is larger than the neural region of interest, as in the ARBS, sSEM, and SCoRe datasets evaluated in this study. In these cases, the data in the statistical report may be filtered to compute local statistics over the region of interest. Such a capability allows for multi-scale study of wide and targeted regions of the brain.

Local Adaptive Thresholding

Key to learning-free segmentation and reconstruction with FLoRIN is the LAT algorithm, based on the method described by Bradley and Roth[43]. As shown in Supplementary Methods: Local Adaptive Thresholding Algorithm, LAT computes the integral image over an arbitrary number of dimensions, allowing for thresholding to incorporate higher-dimensional contextual information such as depth in neural volumes. The threshold computation described by Bradley and Roth is then extended to operate across all dimensions of the computed integral image using the formula described by Tapia[44].

The predecessor to FLoRIN, introduced in Jösch *et al.*[37] used Otsu's method[45] to binarize neural images. Otsu thresholding uses a global value to determine the threshold, making it vulnerable to grayscale shifts and low signal-to-noise ratios. LAT, by contrast, operates on a small neighborhood of voxels at a time, adaptively choosing a threshold for each voxel in the volume. As shown in Supplementary Figure 2, LAT is tolerant to a variety of factors that confound global thresholding methods. Additionally, LAT is significantly faster than global thresholding. We compared the running time against the previous version of the pipeline by segmenting and reconstructing the sSEM volume collected by Jösch *et al.*[37] with FLoRIN and 3D U-Net. As shown in Supplementary Table 1, FLoRIN is an order of magnitude faster than its predecessor due to the change in thresholding

[1] To be released upon publication.

method. Based on both of these findings, we conclude that LAT is primarily responsible for both the increased quality and speed of the FLoRIN pipeline.

μCT X-ray Data Collection

All animal procedures described were performed in accordance with institutional animal care committee regulations. Both of the SRB and ALRB datasets were acquired at the Advanced Photon Source (APS) synchrotron beamline 32-ID-C at Argonne National Laboratory. To minimize the number of artifacts in the tomography the beamline used no optics to filter the X-ray beam. Data acquisition was performed in propagation-based phase contrast mode with 350mm between the detector and sample with a pink beam (δE/E = 102) at 25 keV energy.

Each tomogram was acquired with 1601 projections at different rotation angles equally spaced from 0 to 180 degrees. The projections were acquired with an X-ray to visible light microscope that consists of a scintillator followed by a light microscope. The light is then focused by a Mitutoyo High Resolution 5x objective lens on a 1920×1200 pixel array detector (Point Grey, GS3-U3-23S6M-C) . The numerical aperture of the lens was .21 giving a resolving power of 1.31 μm, the pixel size of the camera was 1.17 μm and the resulting field of view was $2.25 \times 1.41 \text{mm}^2$. Each tomogram took three minutes to be acquired and two minutes to be reconstructed on the Cooley HPC cluster at Argonne National Laboratory. The automatization of the process was done by AuTomo[46] and the final reconstruction by the gridrec algorithm of TomoPy[47]. No phase retrieval was performed.

sSEM Data Collection

Datasets were acquired as described by Jösch *et al.*[37]. Animals were used in accordance with NIH guidelines and protocols approved by Institutional Animal Use and Care Committee at Harvard University. In short, retinas of ChaT-cre mice were anesthetized and infected with rAAV2 expressing APEX2NES under the CAG promoter. 4 weeks following infection, the retina was dissected and fixed with PFA and glutaraldehyde. Following aldehyde fixation, the tissue was washed and reacted with DAB to reveal sites of peroxidase activity. The DAB polymer was subsequently reduced with sodium hydrosulfite, stained with osmium, dehydrated and infiltrated with Durcupan resin. The cured blocks were trimmed and serially sectioned ($\sim$30 nm) using a custom tape collection device (ATUM[38]) attached to a commercial ultramicrotome. Sections were collected on plasma-treated carbon-coated polyamide (Kapton, Sheldahl) 8-mm-wide tape and post-stained with uranyl acetate in maleate and with lead citrate. An automated protocol to locate and image sections on the wafers was used[38] with a Sigma scanning electron microscope (Carl Zeiss), equipped with the ATLAS software (Fibics). Images were acquired using secondary electron detection. Data was then aligned using non-affine alignment through the FijiBento alignment package (https://github.com/Rhoana/FijiBento[37]).

SCoRe Data Collection

All animal procedures were approved by the institutional animal care and use committee at Yale University. Postnatal day 60 male transgenic mice (Thy1-YFPh, Jax 033782) were used for *in-vivo* SCoRe and fluorescence imaging. Mice were anesthetized with Ketamine/Xylazine and a 3mm cranial window was prepared over the somatosensory cortex as previously described[39]. The mice were immediately imaged on a confocal microscope (Leica SP5) with a 20x water immersion objective (1.0NA Leica). For SCoRe imaging, the confocal reflected signals from 488nm, 561nm, and 633nm wavelength lasers were combined into a single image in order to visualize the myelin sheath in a label free fashion[39]. The fluorescence signal from Thy1-YFP labeled axons was collected sequentially in the same cortical region using 488nm wavelength excitation.

Evaluation Metrics

The reconstructions used in this study were evaluated against expert annotations using Hausdorff distance, a similarity measure that determines the maximum distance between any point in the reconstruction and the nearest point in the annotations. Details about this metric may be found in Supplementary Methods: Hausdorff Distance.

Data Availability

The segmentations and reconstructions generated during the current study are available from the corresponding author on reasonable request. The SRB dataset is available for download from the XBrain project. The sSEM volume along with manual annotations, has been published to Dryad[48]. The SCoRe volume used in this study is available from Jaime Grutzendler on reasonable request.

References

1. Perkel, J. M. Life science technologies: This is your brain: Mapping the connectome. *Sci.* **339**, 350–352 (2013).
2. Eyewire. http://eyewire.org/explore (2014).
3. Giuly, R. J., Kim, K.-Y. & Ellisman, M. H. Dp2: Distributed 3d image segmentation using micro-labor workforce. *Bioinforma.* **29** (2013).

4. Knowles-Barley, S. *et al.* Mojo 2.0: Connectome annotation tool. *Front. Neuroinformatics* **60** (2013).

5. Saalfeld, S., Cardona, A., Hartenstein, V. & Tomančák, P. Catmaid: collaborative annotation toolkit for massive amounts of image data. *Bioinforma.* **25**, 1984–1986 (2009).

6. Helmstaedter, M., Briggman, K. L. & Denk, W. High-accuracy neurite reconstruction for high-throughput neuroanatomy. *Nat. Neurosci.* **14**, 1081–1088 (2011).

7. Jeong, W.-K. *et al.* Ssecrett and neurotrace: interactive visualization and analysis tools for large-scale neuroscience data sets. *IEEE Comput. Graph. Appl.* **30**, 58–70 (2010).

8. Cardona, A. *et al.* TrakEM2 software for neural circuit reconstruction. *PLoS One* **7**, e38011 (2012).

9. Yushkevich, P. A. *et al.* User-guided 3d active contour segmentation of anatomical structures: significantly improved efficiency and reliability. *Neuroimage* **31**, 1116–1128 (2006).

10. Takemura, S.-y. *et al.* A visual motion detection circuit suggested by drosophila connectomics. *Nat.* **500**, 175–181 (2013).

11. Holcomb, P. S. *et al.* Synaptic inputs compete during rapid formation of the calyx of held: a new model system for neural development. *The J. Neurosci.* **33**, 12954–12969 (2013).

12. Kroeger, T., Mikula, S., Denk, W., Koethe, U. & Hamprecht, F. A. Learning to segment neurons with non-local quality measures. In *Medical Image Computing and Computer-Assisted Intervention*, 419–427 (2013).

13. Narasimha, R., Ouyang, H., Gray, A., McLaughlin, S. W. & Subramaniam, S. Automatic joint classification and segmentation of whole cell 3D images. *Pattern Recognit.* **42**, 1067–1079 (2009). DOI 10.1016/j.patcog.2008.08.009.

14. Tan, X. & Sun, C. Membrane extraction using two-step classification and post-processing. In *Proc. of ISBI* (2012).

15. Lucchi, A. *et al.* Learning structured models for segmentation of 2-D and 3-D imagery. *IEEE Transactions on Med. Imaging* **34**, 1096–1110 (2015).

16. Tong, S. & Koller, D. Support vector machine active learning with applications to text classification. *J. Mach. Learn. Res.* **2**, 45–66 (2001).

17. Mahapatra, D. & Buhmann, J. Visual Saliency Based Active Learning for Prostate MRI Segmentation. *Signal Process. Mag. IEEE* **27**, 25–38 (2010). URL citeulike-article-id:7359849://dx.doi.org/10.1109/msp.2010.936730. DOI doi: 10.1109/msp.2010.936730.

18. Kreshuk, A. *et al.* Automated tracing of myelinated axons and detection of the nodes of Ranvier in serial images of peripheral nerves. *J. Microsc.* **259**, 143–154 (2015). DOI 10.1111/jmi.12266.

19. R, A. & GA, A. Towards the automatic classification of neurons. *Trends Neurosci.* **38**, 307–318 (2015). DOI 10.1016/j.tins.2015.02.004.

20. Liu, T., Jones, C., Seyedhosseini, M. & Tasdizen, T. A modular hierarchical approach to 3D electron microscopy image segmentation. *J. Neurosci. Methods* **226**, 88–102 (2014). URL http://dx.doi.org/10.1016/j.jneumeth.2014.01.022. DOI 10.1016/j.jneumeth.2014.01.022. NIHMS150003.

21. Kaynig, V. *et al.* Large-scale automatic reconstruction of neuronal processes from electron microscopy images. *Med. Image Anal.* **22**, 77–88 (2015). DOI 10.1016/j.media.2015.02.001. 1303.7186.

22. Uzunbas, M. G., Chen, C. & Metaxas, D. An efficient conditional random field approach for automatic and interactive neuron segmentation. *Med. Image Anal.* **27**, 31–44 (2016). URL http://dx.doi.org/10.1016/j.media.2015.06.003. DOI 10.1016/j.media.2015.06.003.

23. Haehn, D. *et al.* Design and evaluation of interactive proofreading tools for connectomics. *IEEE Trans. Vis. Comput. Graph.* **20**, 2466–2475 (2014). DOI 10.1109/TVCG.2014.2346371.

24. Jones, C., Liu, T., Cohan, N. W., Ellisman, M. & Tasdizen, T. Efficient semi-automatic 3D segmentation for neuron tracing in electron microscopy images. *J. Neurosci. Methods* **246**, 13–21 (2015). URL http://dx.doi.org/10.1016/j.jneumeth.2015.03.005. DOI 10.1016/j.jneumeth.2015.03.005.

25. Jurrus, E. *et al.* Detection of neuron membranes in electron microscopy images using a serial neural network architecture. *Med. Image Anal.* **14**, 770–783 (2010). URL http://dx.doi.org/10.1016/j.media.2010.06.002. DOI 10.1016/j.media.2010.06.002.

26. Huang, G. B. & Jain, V. Deep and wide multiscale recursive networks for robust image labeling. *arXiv preprint arXiv:1310.0354* (2013).

27. Lee, K., Zlateski, A., Vishwanathan, A. & Seung, H. S. Recursive Training of 2D-3D Convolutional Networks for Neuronal Boundary Detection. *arXiv.org* 1–10 (2015). URL http://arxiv.org/abs/1508.04843. 1508.04843.

28. Ciresan, D., Giusti, A., Gambardella, L. M. & Schmidhuber, J. Deep neural networks segment neuronal membranes in electron microscopy images. In *Advances in Neural Information Processing Systems 25*, 2843–2851 (2012).

29. Gray Roncal, W. *et al.* VESICLE : Volumetric Evaluation of Synaptic Interfaces using Computer vision at Large Scale. *Br. Mach. Vis. Conf.* 1–9 (2015). 1254329.

30. Kasthuri, N. *et al.* Saturated reconstruction of a volume of neocortex. *Cell* **162**, 648–661 (2015).

31. Kaynig, V. *et al.* Large-scale automatic reconstruction of neuronal processes from electron microscopy images. *Med. Image Analysis* **22**, 77–88 (2015).

32. Wernitznig, S. *et al.* Optimizing the 3D-reconstruction technique for serial block-face scanning electron microscopy. *J. Neurosci. Methods* **264**, 16–24 (2016). URL http://dx.doi.org/10.1016/j.jneumeth.2016.02.019. DOI 10.1016/j.jneumeth.2016.02.019.

33. Ronneberger, O., Fischer, P. & Brox, T. U-net: Convolutional networks for biomedical image segmentation. In *International Conference on Medical Image Computing and Computer-Assisted Intervention*, 234–241 (Springer, 2015).

34. Çiçek, Ö., Abdulkadir, A., Lienkamp, S. S., Brox, T. & Ronneberger, O. 3d u-net: learning dense volumetric segmentation from sparse annotation. In *International Conference on Medical Image Computing and Computer-Assisted Intervention*, 424–432 (Springer, 2016).

35. Milletari, F., Navab, N. & Ahmadi, S.-A. V-net: Fully convolutional neural networks for volumetric medical image segmentation. In *3D Vision (3DV), 2016 Fourth International Conference on*, 565–571 (IEEE, 2016).

36. Chklovskii, D. B., Vitaladevuni, S. & Scheffer, L. K. Semi-automated reconstruction of neural circuits using electron microscopy. *Curr. Opin. Neurobiol.* **20**, 667–675 (2010). URL http://dx.doi.org/10.1016/j.conb.2010.08.002. DOI 10.1016/j.conb.2010.08.002.

37. Joesch, M. *et al.* Reconstruction of genetically identified neurons imaged by serial-section electron microscopy. *eLife* **5**, e15015 (2016).

38. Hayworth, K. J. *et al.* Imaging atum ultrathin section libraries with wafermapper: a multi-scale approach to em reconstruction of neural circuits. *Front. Neural Circuits* **8**, 1–18 (2014).

39. Schain, A. J., Hill, R. A. & Grutzendler, J. Label-free in vivo imaging of myelinated axons in health and disease with spectral confocal reflectance microscopy. *Nat. medicine* **20**, 443–449 (2014).

40. Dyer, E. L. *et al.* Quantifying mesoscale neuroanatomy using x-ray microtomography. *eNeuro* **4**, ENEURO–0195 (2017).

41. da Costa, N. M. & Martin, K. A. Sparse reconstruction of brain circuits: or, how to survive without a microscopic connectome. *Neuroimage* **80**, 27–36 (2013).

42. Lam, S. S. *et al.* Directed evolution of apex2 for electron microscopy and proximity labeling. *Nat. Methods* **12**, 51 (2015).

43. Bradley, D. & Roth, G. Adaptive thresholding using the integral image. *J. graphics, gpu, game tools* **12**, 13–21 (2007).

44. Tapia, E. A note on the computation of high-dimensional integral images. *Pattern Recognit. Lett.* **32**, 197–201 (2011).

45. Otsu, N. A threshold selection method from gray-level histograms. *Autom.* **11**, 23–27 (1975).

46. Du, M. *et al.* An automated pipeline for the collection, transfer, and processing of large-scale tomography data. In *OSA Biophotonics Congress* (2018).

47. Gürsoy, D., De Carlo, F., Xiao, X. & Jacobsen, C. Tomopy: a framework for the analysis of synchrotron tomographic data. *J. synchrotron radiation* **21**, 1188–1193 (2014).

48. Joesch, M. *et al.* Data from: Reconstruction of genetically identified neurons imaged by serial-section electron microscopy (2016). URL https://doi.org/10.5061/dryad.h67t6. DOI doi:10.5061/dryad.h67t6.

Acknowledgements

Ali Shahbazi, Jeffery Kinnison, Walter Scheirer, Rafael Vescovi, and Narayanan Kasthuri were supported by the Office of the Director of National Intelligence (ODNI), Intelligence Advanced Research Projects Activity (IARPA) under contract #D16PC00002. Marc Takeno, and Nuno M. da Costa were supported by IARPA via Department of Interior/ Interior Business Center (DoI/IBC) contract number #D16PC00004. The views and conclusions contained herein are those of the organizers and should not be interpreted as necessarily representing the official policies, either expressed or implied, of ODNI, IARPA, DoI/IBC, or the U.S. Government. The U.S. Government is authorized to reproduce and distribute reprints for governmental purposes notwithstanding any copyright annotation therein. Equipment was generously donated by the NVIDIA Corporation.

Author Contributions Statement

A.S. and J.K. developed the FLoRIN framework and carried out all segmentation and reconstruction processes. W.S. designed and led the research. R.V, M.D., and B.K. provided the SRB μCT X-ray data used in this study. M.T., H.Z., an N.C. provided the ALRB μCT X-ray data used in this study M.J. provided the sSEM data used in this study. R.H. and J.G. provided the SCoRe data used in this study. All authors contributed to the text of the manuscript.

Additional information

The authors declare no competing financial interests.

Table 1. Evaluation of μCT X-ray reconstructions imaged at $1.2\,\mu$m resolution against expert annotations.

	Runtime (minutes)			Hausdorff Distance			Number of Cells		Average Minimum Intercellular Dist. (vx)	
	2D FLoRIN	3D FLoRIN	3D U-Net	2D FLoRIN	3D FLoRIN	3D U-Net	2D FLoRIN	3D FLoRIN	2D FLoRIN	3D FLoRIN
RBS	0.15	0.32	172.74	6.37×10^{-3}	1.59×10^{-3}	5.86×10^{-3}	321	321	71.30	69.59
ARBS	27.99	47.5	-	-	-	-	124,948	124,948	72.98	73.56

Table 2. Evaluation of sSEM reconstructions against expert annotations.

	Runtime (minutes)		Hausdorff Distance		Variation of Information	Recall
	2D FLoRIN	3D FLoRIN	2D FLoRIN	3D FLoRIN	2D FLoRIN	2D FLoRIN
SubVol 1	16.82	16.56	2.51×10^{-4}	3.24×10^{-4}	0.6841	98.63%
SubVol 2	46.3	73.29	8.20×10^{-4}	6.36×10^{-4}	0.7066	93.03%

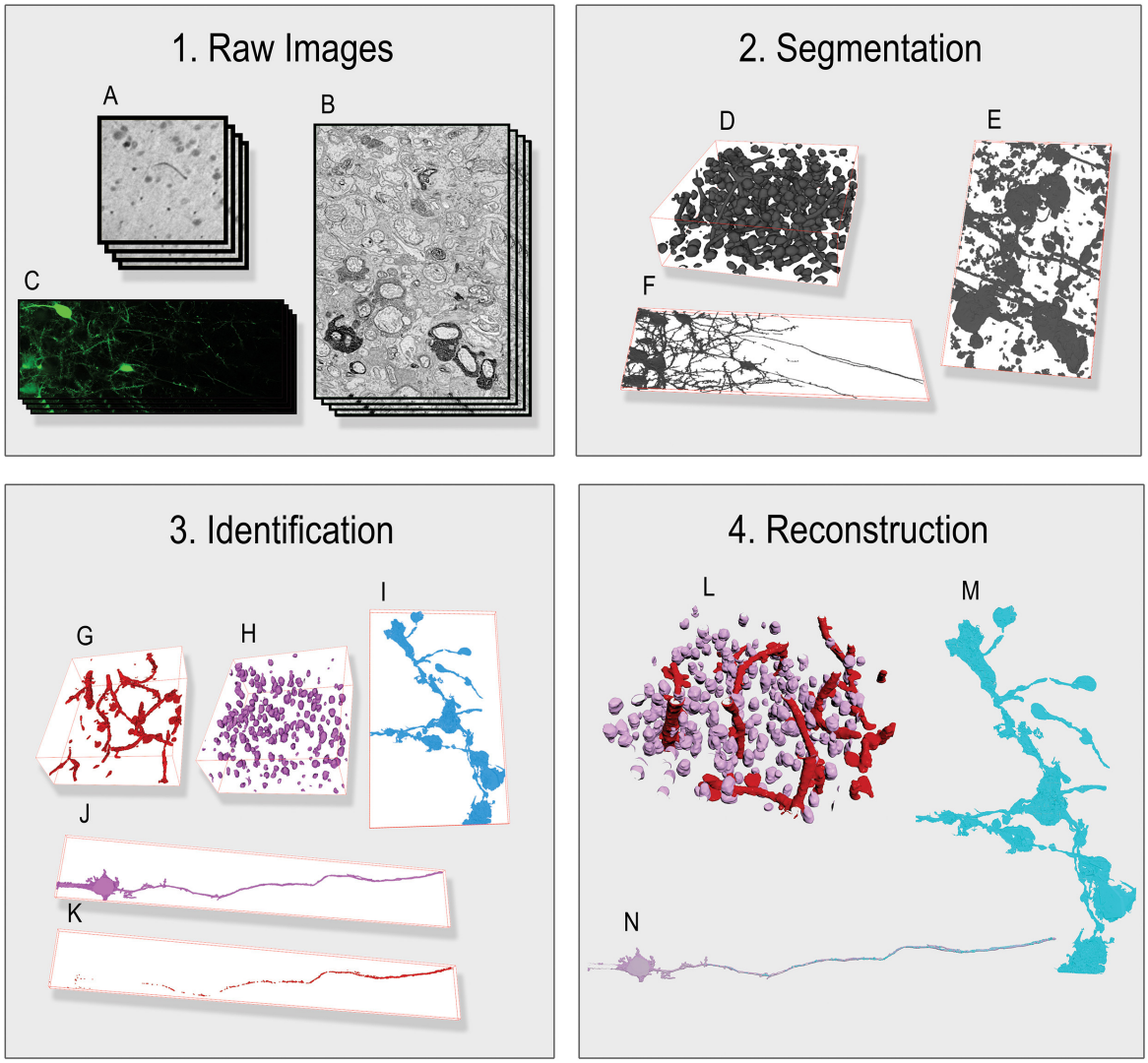

Figure 1. The Flexible Learning-Free Reconstruction of Neural Circuits (FLoRIN) pipeline is software for sparse segmentation and reconstruction of neural volumes. Unlike current methods that rely on learned models, FLoRIN uses classical learning-free image processing and computer vision methods to quickly and effectively segment and reconstruct microstructures in microscopic images. The FLoRIN pipeline consists of the following steps: (1) Raw images are loaded into the pipeline. (2) Images are segmented using Local Adaptive Thresholding to binarize structures of interest. (3) Connected components in the binarized images are filtered to remove noise and distinguish between classes of microstructures. (4) Each class of microstructure is saved in its own volume and a statistical report is generated based on the location, geometry, and grayscale histogram of each individual structure. By virtue of being learning-free, FLoRIN is generalizable across multiple imaging modalities, including μCT X-ray (A, D, G, H, L), sSEM (B, E, I, M), and SCoRe (C, F, J, K, N) images.

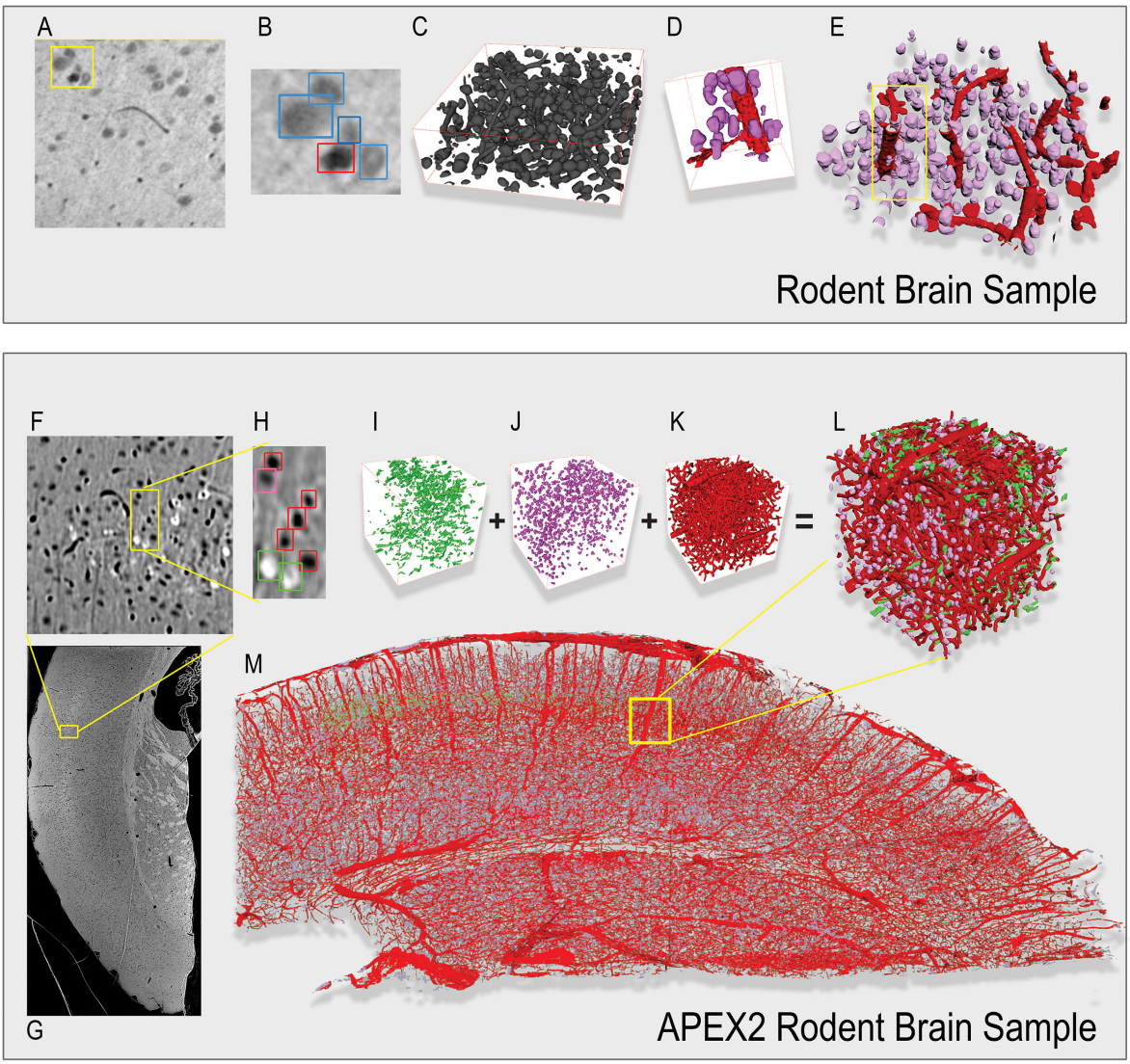

Figure 2. FLoRIN reconstructions of the Rodent Brain Sample (RBS) (top) and APEX2-labeled Rodent Brain Sample (ARBS) (bottom) μCT X-ray volumes. (A) Within the RBS volume, cells and vasculature are visually distinct in the raw images, with vasculature appearing darker than cells. (B) Individual microstructures may be extremely close (such as the cells and vasculature in this example), making reconstruction efforts prone to merge errors. (C) Segmentation by FLoRIN extracts the miscrostructures from the images with minor noise and artifacts that are much smaller than the structures of interest. (D) FLoRIN is able to separate nearby microstructures based on geometric and grayscale features. (E) After filtering, the final reconstruction distinguishes between cells (purple) and vasculature (red). (F) The ARBS volume spans a large portion of the rodent brain. (G, H) In addition to non-APEX cells and vasculature, ARBS contains APEX2-labeled cells that appear lighter than the background. FLoRIN segmented and filtered the APEX2-labeled cells (I), non-APEX cells (J), and vasculature (K), then reconstructed them into a single volume (L). (M) Throughout the ARBS volume, the vasculature was segmented as a single connected component, and FLoRIN discovered 123,424 non-APEX2-labeled cells and 1,524 APEX2-labeled cells.

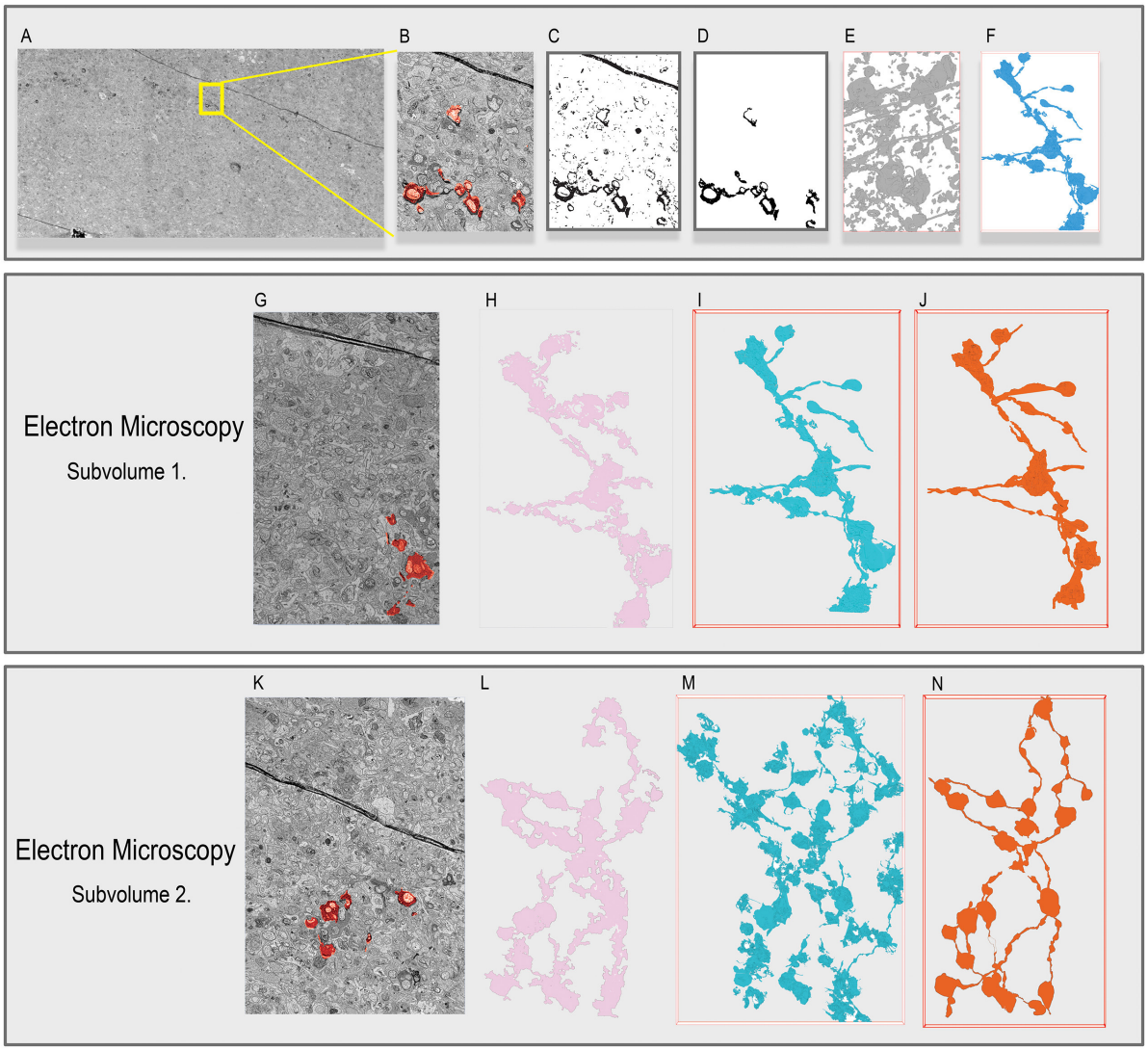

Figure 3. (A, B) The APEX2 positive sSEM sample contains a number of APEX-labeled SAC cells with annotated dendritic branches. The FLoRIN pipeline can conduct Segmentation and Filtering in 2D (C, D) or 3D (E, F). Segmentation (C, E) captures extraneous information, including non-APEX processes and artifacts, and these are removed in the Filtering stage (D, F). The middle panel shows (G) a sample of Subvolume 1 of the APEX2 positive sSEM sample, (H) the 2D reconstruction created by 2D FLoRIN, (I) the 2D reconstruction created by 3D FLoRIN, (J) ground-truth annotations of the APEX-labeled SAC cells. Both FLoRIN methods were able to reconstruct the annotated regions with many of the processes. While the 2D FLoRIN reconstruction incurred a number of merge errors on collapsing the reconstruction into a single plane, many of these issues are handled by 3D FLoRIN filtering connected components based on volumetric information. The bottom panel shows (K) a sample of Subvolume 2 of the APEX2 positive sSEM sample, (L) the 2D reconstruction created by 2D FLoRIN, (M) the 2D reconstruction created by 3D FLoRIN, (N) ground-truth annotations of the APEX-labeled SAC cells. Due to fewer artifacts in this subvolume, the two FLoRIN methods captured roughly the same information. Notably, though, 3D FLoRIN discovered additional pieces of the APEX2 positive process in this subvolume that were not present in the ground-truth data.

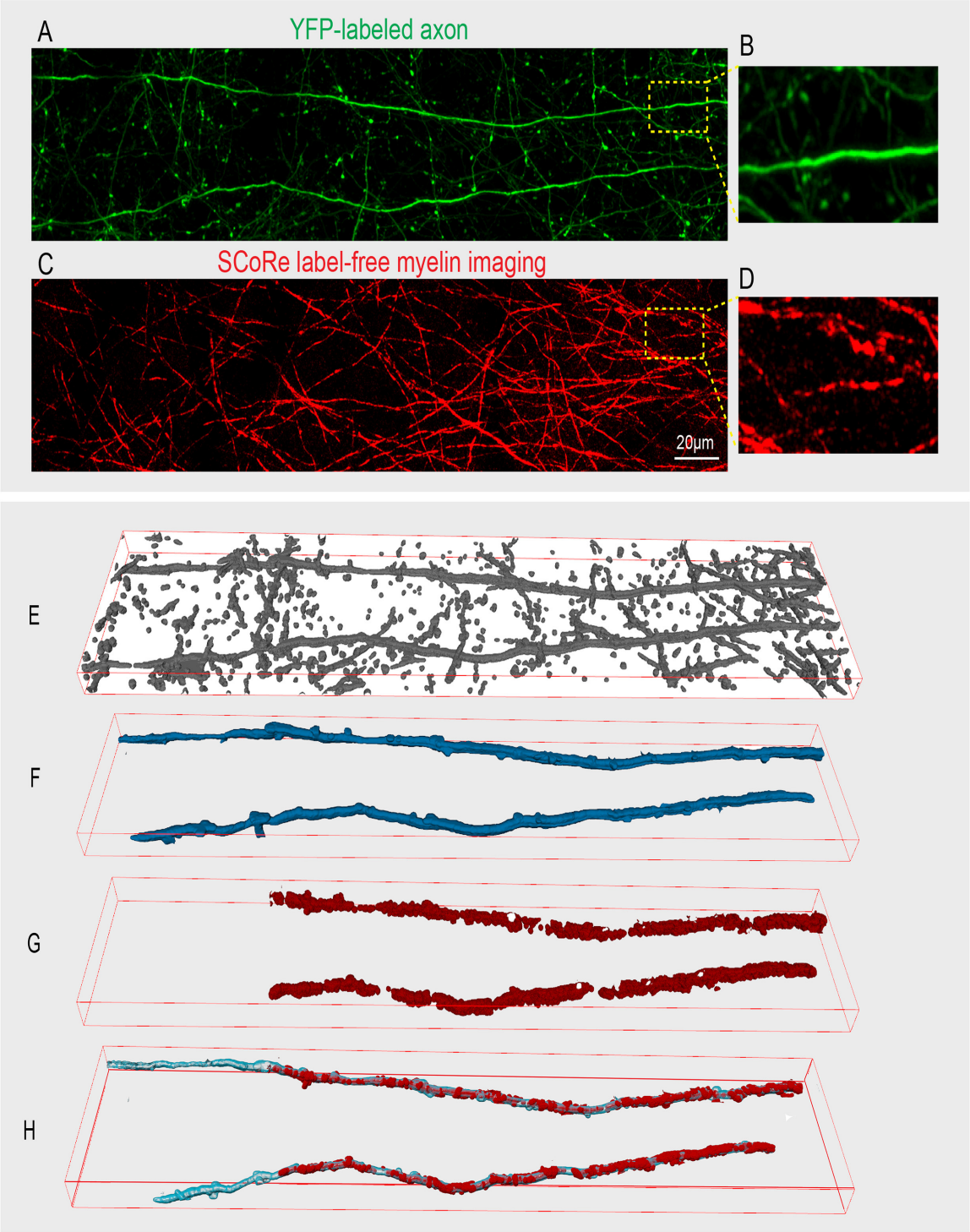

Figure 4. The SCoRE modality represents *in-vivo* (A-B) images captured from the cerebral cortex of a live mouse showing confocal fluorescence signals from Thy1-YFP labeled axons. (C-D) Label-free SCoRe images captured from the same region showing single myelinated fibers. (E) FLoRIN segmented axons generated using YFP signal. (F) Automated isolation and reconstruction of two YFP labeled axons within the volume. (G) corresponding SCoRe signals overlapping with the reconstructed axons. (H) Final reconstructed myelinated axons revealing unmyelinated and myelinated portions of the reconstructed axons.